Simulation of the surface structure of lithium manganese oxide spinel

R. Benedek and M. M. Thackeray

Chemical Sciences and Engineering Division, Argonne National Laboratory, Argonne, Illinois 60439, USA

(Received 21 April 2010; revised manuscript received 27 October 2010; published 31 May 2011)

Simulations of the surface structure of low-index surfaces of $LiMn_2O_4$ (LMO), a candidate Li-ion battery electrode material, have been performed within the GGA + U approximation, using the VASP code. Surfaces of (001), (110), and (111) orientation were considered, with at least two terminations treated in each case. A slab geometry was employed, with termination-layer vacancies introduced to remove the bulk dipole moment while maintaining ideal stoichiometry. To complement static-structure relaxation calculations, molecular-dynamics simulations were performed to explore the phase space of possible surface reconstructions. A reconstruction is predicted for the Mn-terminated (111) surface, in which the top layers mix in stoichiometric proportions to form an LMO termination layer with square-planar-coordinated Mn. Average surface Mn oxidation states are reduced, relative to the bulk, for all surfaces considered, as a consequence of the lower-energy cost of Jahn-Teller distortion at the surface. Threefold-coordinated surface Mn, found for two terminations, is divalent, which may enhance its vulnerability to dissolution. The Li-terminated (001) surface is lowest in energy, consistent with previous classical-potential simulations for $MgAl_2O_4$ that showed the Mg-terminated (001) surface to be lowest in energy.

DOI: 10.1103/PhysRevB.83.195439 PACS number(s): 68.35.B−, 68.47.Gh

I. INTRODUCTION

Lithium manganese oxide spinel $LiMn_2O_4$ (LMO) is a candidate electrode material for lithium-ion batteries.[1] At room temperature, LMO adopts the same cubic crystal structure as the prototype spinel, $MgAl_2O_4$, with symmetry $Fd\bar{3}m$. As for many ternary oxides, however, the surface atomic structure is poorly known for LMO. Characterization of the surface and interfacial structures of LMO would be a step toward understanding its chemical and electrochemical reactions. The significance of surface and interface properties is further accentuated by the focus on nanostructured electrodes,[2] which shorten Li diffusion paths.

Among direct spinel-structured surfaces, that of magnesium aluminum oxide has perhaps received the most theoretical attention. Atomic-scale simulations were performed of low-index surfaces of $MgAl_2O_4$, based on semiempirical interatomic potentials.[3,4] Cation terminations for the low-energy orientation, (001), have been simulated with density functional theory.[5] The (111) orientation was found to exhibit the most extensive atomic rearrangements at the surface.

Compared to $MgAl_2O_4$, LMO has the extra complications of Mn disproportionation and Jahn-Teller activity of the trivalent ions. These features are amenable to simulation at the GGA + U level of density functional theory.[6,7] Previous first-principles simulations of the surface structure of $LiMn_2O_4$, however, appear limited to a recent investigation of the (001) surface.[8]

In this paper, we present simulations of essentially all low-index surfaces of $LiMn_2O_4$ using the GGA + U method, as implemented in the VASP code[9–11] with projector-augmented wave (PAW) pseudopotentials. This work is intended to provide insight into surface atomic structure and atomic structure data that may be employed in future simulations of dissolution of lithium manganate spinel in acid.[12,13] The atomic structure input data may also provide input for simulations of lithium manganate interfaces, for example with protective coatings[14] or electrolyte.

A periodically repeating slab geometry is convenient for surface calculations. Since the low-index orientations are polar (Tasker type III[15]), an unphysical dipole moment perpendicular to the slab occurs unless surface defects (e.g., vacancies), surface electronic states, or other reconstructions are introduced.[16] To reduce the computational burden, only compositions with ideal stoichiometry (canonical ensemble) are considered in this work. Ideal stoichiometry is maintained by transferring atoms from one surface of the slab to the opposite surface.[17]

Given the variety of terminations that are possible, the identification of common features of lithium manganate surfaces is of particular interest. In this work, we consider all low-index surface terminations derived from a symmetry plane (so that the slab may be constructed with essentially identical top and bottom surfaces), and, additionally, the oxygen-terminated (111) surface, which is asymmetrical. This set of seven terminations [two (001), two (110), and three (111)] is sufficient to reveal some pervasive features of lithium manganate spinel free surfaces, including the reduced average oxidation state of Mn ions near the surface, the presence of Mn coordination numbers that range from 3 to 5 (in contrast to octahedral coordination in the bulk), and the absence of nonbridging (singly coordinated) oxygen at flat surfaces.

In recent years, first-principles simulations of several binary oxide surfaces, such as MnO,[18] have been performed as a function of oxygen partial pressure within the grand canonical ensemble. In such simulations, a small number of candidate reconstructions is identified, and the surface free energy is evaluated for each. A recent grand canonical ensemble surface simulation has been performed for the ternary, $LiCoO_2$.[19] For many ternaries, however, the large number and complexity of candidate reconstructions may make this approach prohibitive, and the present work is performed within the canonical ensemble. In this work, instead of attempting to select relevant candidate surface structures, we employ first-principles molecular dynamics to explore the phase space of possible

reconstructions. In the case of the Mn-terminated (111) surface, an atomic rearrangement and ordering was found in which the three components are mixed to form a composite stoichiometric surface layer with square-planar coordination of Mn ions in the surface plane. Direct experimental tests of this prediction are not presently available. The prediction suggests, however, that the bulk-terminated surface is highly unstable, and that extensive atomic rearrangements of (111) surfaces are likely.

In the analysis presented in the following sections, we focus on surface Mn oxidation states and coordination numbers, which are relevant to the surface reactions of lithium manganate, to be addressed in future work. We consider here only pristine surfaces, although hydroxylation is a ubiquitous feature of real surfaces.[20] Despite the difficulty of measurements, pristine surfaces are an important benchmark for simulation.

II. SLAB REPRESENTATION OF LITHIUM MANGANATE SURFACES

We outline here the construction of bulk-terminated slabs, which are employed as (pre-relaxation) input atomic position data in the VASP calculations. The degrees of freedom of the slab include (a) the surface orientation, (b) the termination plane, (c) the size of the slab unit cell parallel and perpendicular to the surface (slab thickness), and (d) the configuration of surface vacancies, introduced to cancel the surface dipole moment,[16,17] which would otherwise result in energy divergences for Tasker type III surfaces in the limit of thick slabs. We consider the low-index surface orientations (001), (110), and (111). Specification of the degrees of freedom (b)–(d) is described in the following subsections.

A. Slab layer sequences

All surface terminations obtained from symmetrical cleavage planes for low-index surfaces are considered in this work. In addition, asymmetrical O-terminated surfaces for the (111) surface are addressed. Altogether, two (001) terminations, two (110) terminations, and three (111) terminations are considered. For slab terminations associated with symmetrical cleavage planes, the macroscopic electrostatic dipole moment is automatically canceled when half of the atoms in the bulk termination layer are assigned to the top and half to the bottom layer of the slab, which results in a termination layer vacancy concentration $C_v = 1/2$. For slabs derived from asymmetric cleavage planes, a different vacancy concentration is required to cancel the macroscopic dipole moment.[17]

The underlying layer sequences for low-index orientations, from which the various terminations are derived, are reviewed in the following subsections.

1. (111) surface

(111) atomic layers in bulk $LiMn_2O_4$ follow the sequence (...M_3;O_4;L,M,L;O_4;M_3...), where the relative layer atomic density is indicated by the subscripts; for example, the M_3 layers have 3/4 as many atoms per unit layer area as the O_4 layers. M occupies octahedral sites in the M_3 layers. Since the LML triple cation layers (with tetrahedral L and octahedral M) are closely spaced, we regard them as sublayers of a single composite layer. (Semicolons separate distinct layers and commas separate sublayers of the LML composite layer.)

Two symmetry planes occur in the (111) layer sequence, both of which correspond to Mn-bearing termination surfaces. The cleavage plane in one case is at a pure Mn layer sandwiched between oxygen layers, and in the other is at the center of an LML composite layer. The layer sequence for the first such termination (at ideal stoichiometry) is

$$[(1-C_v)\mathrm{M_3;O_4;L,M,L;O_4;M_3;O_4,L,M,L;}\ldots\mathrm{O_4;}C_v\mathrm{M_3}]. \quad (1)$$

The (stoichiometry-conserving) termination layer compositions include the factors $1 - C_v$ and C_v on the top and bottom of the slab, respectively, where $C_v = 1/2 (1 - C_v = 1/2)$ are the vacancy concentration at the top (bottom) of the slab.

The resultant sequence may be regarded as a stacking of stoichiometric, zero-dipole-moment ($1/2M_3$;O_4;L,M,L;O_4;$1/2M_3$) units perpendicular to the plane of the surface. The slab obtained by the stacking of such units can be viewed as a minimally reconstructed surface: atoms are in bulk-terminated sites, with a configuration of vacancies in the termination layer. More general reconstructions[16] that would involve, e.g., additional surface vacancies are not considered in the present work.

As mentioned above [item (c)], the size of the unit cell parallel and perpendicular to the surface, e.g., the number of such stacking units perpendicular, n_{perp}, and parallel, n_{par}, to the surface, must be specified to fix the number of degrees of freedom for the slab. The minimal value of n_{par} is 2 in this case, to give integral numbers of atoms in the (top and bottom) terminating layers of the periodic unit cell of the slab.

The sequence of layers for cleavage at the (L,M,L) layer is

$$(1/2\mathrm{M,L;O_4;M_3;O_4;L,M,L;}\ldots\mathrm{,M_3;O_4;L,}1/2\mathrm{M}), \quad (2)$$

and the corresponding stoichiometric stacking unit is ($1/2$M,L;O_4;M_3;O_4;L,$1/2$M).

A stoichiometric slab terminated at the oxygen layer has the sequence

$$(1-C_v)\mathrm{O_4;L,M,L;O_4;M_3;O_4;L,M,L;}\ldots\mathrm{O_4;}\ldots\mathrm{M_3;}C_v\mathrm{O_4}. \quad (3)$$

Since cleavage is at an asymmetrical plane in this case, the dipole-moment canceling value[17] of C_v deviates from one-half. If we assume (bulk average) charges of -2, $+3.5$, and $+1$ on oxygen ions, Mn ions, and Li ions, respectively, we obtain $C_v = 0.3125$. Therefore, $C_v \approx 5/8$ and three of eight oxygen sites are left vacant in the termination layer above a Mn layer, and five oxygen sites are vacant at the opposite termination layer.

The initial atomic coordinates for a bulk-terminated slab can be fixed by specifying the termination, the slab size parameters n_{perp} and n_{par}, and the vacancy arrangement of the terminating layers. For (111) slabs, we have selected $n_{\mathrm{perp}} = 3$ and $n_{\mathrm{par}} = 2$. Since the stacking unit given above contains two $LiMn_2O_4$ formula units, the periodic unit of each such slab contains $2 \times 3 \times 2 = 12$ formula units, or 84 atoms. The selected unit-cell vectors $A1$ and $A2$ parallel to the surface and the termination layer vacancy configuration for the (M;O)

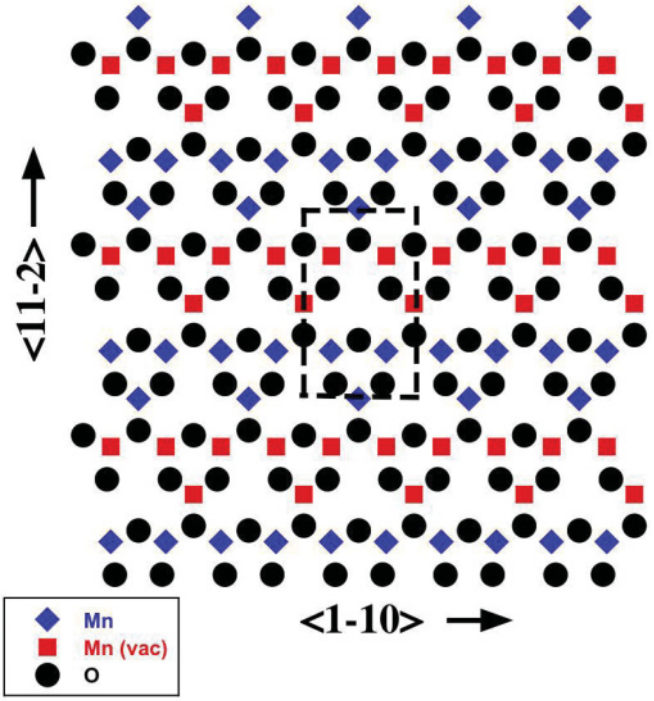

FIG. 1. (Color online) Unreconstructed surface unit cell for a (111) slab. The boundaries of the computational unit cell are indicated by dashed lines. Diamonds denote surface layer Mn atoms and squares Mn vacancies (or vice versa); O atoms in the layer below the terminating layer are represented by filled circles. Owing to the Mn surface vacancies, some O atoms are singly bonded (nonbridging), with no bonds to the termination layer. No nonbridging oxygen ions remain in the relaxed structure.

termination are illustrated in Fig. 1. The initial configuration of vacancies is chosen so as to minimize the deficit of M-O bonds at the surface;[19] this choice is not necessarily unique, however.

2. (001) surface

The layer sequence for a slab with (001) orientation may be regarded as an alternation between M_4O_8 and L_2 layers, and each type of layer is a possible symmetric cleavage plane. The layer sequence for the MO termination is thus

$$1/2(M_4O_8); L_2; M_4O_8; L_2; \ldots, 1/2(M_4O_8) \quad (4)$$

and the stoichiometric stacking unit is $1/2(M_4O_8);L_2;1/2(M_4O_8)$. The sequence for the L termination is

$$1/2(L_2); M_4O_8; L_2; \ldots, M_4O_8; 1/2(L_2). \quad (5)$$

The termination-layer unit cell employed for the MO termination is illustrated in Fig. 2. To test the convergence of the calculations with slab thickness, calculations were performed for two slab thicknesses, for the MO termination, with $n_{\text{perp}} = 4$ and 8, which correspond to 56- and 112-atom unit cells, respectively. The larger of these corresponds essentially to the cell size employed by Ouyang *et al.*[8]

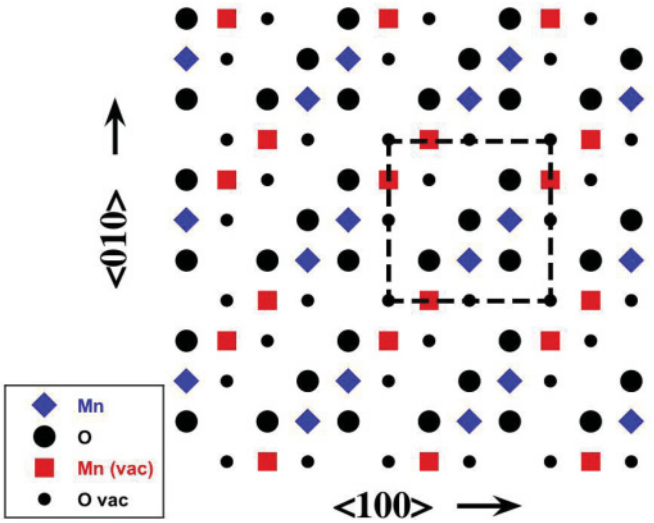

FIG. 2. (Color online) Unrelaxed surface unit cell of a (001) slab with MO termination. The dimensions of the periodic unit cell are indicated by dashed lines. Large (small) diamonds (squares) denote termination layer Mn atoms (Mn vacancies); O atoms (vacancies) are represented by large (small) filled circles.

3. (110) surface

An alternation occurs between LMO_2 and MO_2 layers in slabs with (110) orientation, each of which presents a symmetric cleavage plane. Thus the sequence for the MO termination is

$$1/2(MO_2), LMO_2, \ldots, 1/2(MO_2), \quad (6)$$

and the stoichiometric stacking unit is $1/2(MO_2);LMO_2;1/2(MO_2)$. The termination-layer unit cell for the MO termination is illustrated in Fig. 3. (110) surface calculations were performed for 84-atom unit-cell slabs.

III. METHOD OF CALCULATION

The GGA + U approximation was employed in this work, as implemented in the VASP code, version 4.6,[9–11] with the PW91 exchange-correlation potential,[21] and effective Coulomb interaction parameter $U_{\text{eff}} = 4.84$ eV.[6] The Hellmann-Feynman forces obtained from the Kohn-Sham orbitals are employed either in atomic relaxation calculations by the conjugate gradient method, or in first-principles molecular-dynamics simulations.

Slab unit-cell atomic arrangements were constructed, as outlined in the previous section, for three low-index orientations of $LiMn_2O_4$, with initial atomic coordinates taken from bulk calculations. Lattice basis vectors parallel to slab layers were chosen to be consistent with (calculated) bulk cubic crystal lattice parameters.[13] Bulk $LiMn_2O_4$ is cubic at room temperature, although symmetry-lowering phase transitions occur at lower temperatures.[22] Adjacent slabs are separated in the perpendicular direction by a 1 nm vacuum layer. For simplicity, ferromagnetic spin ordering is considered. The relaxation calculations were performed with the 500-eV high-precision setting. In most of the calculations, a single k point gave satisfactory convergence for the present purposes,

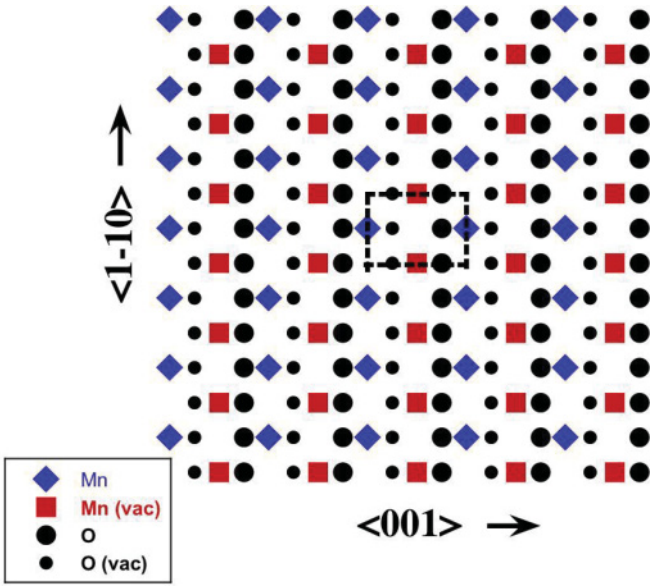

FIG. 3. (Color online) Unrelaxed surface unit cell of a (110) slab with MO termination. The dimensions of the periodic unit cell are indicated by dashed lines. Large (small) diamonds denote termination layer Mn atoms (Mn vacancies); O atoms (vacancies) are represented by large (small) filled circles.

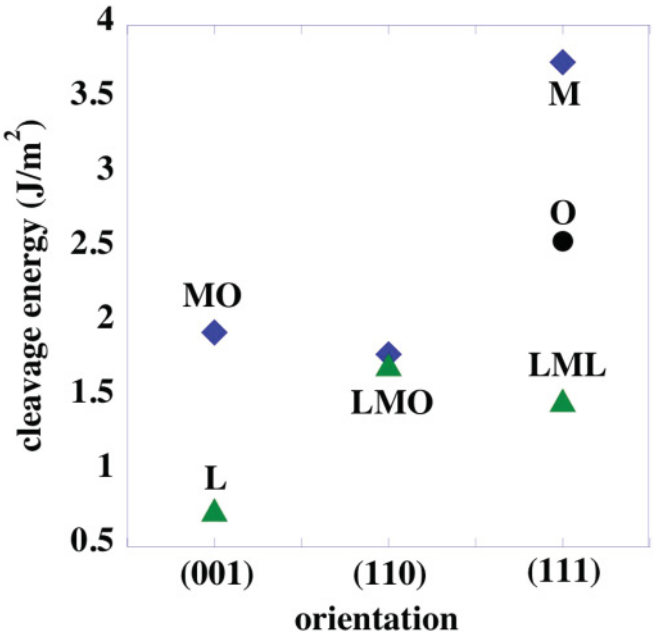

FIG. 4. (Color online) Calculated cleavage energies for low-index surfaces of lithium manganate.

although some tests were done with larger k-point sets. The first-principles molecular-dynamics simulations for the (111) oriented slab were performed at the low-precision setting (energy cutoff 300 eV) with a single k point. Since Mn ions are invariably in a high-spin state, the magnetic moment reveals the oxidation state.

The initial relaxation calculation for each slab was performed with conjugate gradients. First-principles molecular-dynamics thermalization simulations at 300 K were then performed for a simulation time of the order of 1 ps on the relaxed slabs to minimize the likelihood of trapping in a local energy minimum configuration. Conjugate gradient relaxation was then alternated with first-principles molecular-dynamics simulation until a relatively low-energy plateau was reached, and the atomic structure was reasonably well converged; structural convergence may require a long simulation time. In the case of the Mn-terminated (111) surface, which exhibited the most extensive atomic rearrangement, the MD simulation was continued for a total time of about 10 ps. For the (001) and (110) surfaces, the thermalization–conjugate-gradient steps did not appreciably lower the energy, or change the structure, from that obtained in the initial relaxation.

IV. RESULTS

A. Cleavage energy

The cleavage energy [energy difference between the slab with atoms in (unrelaxed) bulk-terminated sites, and the perfect crystal energy, normalized to the surface area] is a measure of the relative stability of different surface orientations and terminations. Cleavage energies for the seven terminations under consideration are plotted in Fig. 4. The relative magnitude of the various energies can be rationalized to some extent by counting broken bonds. For example, the vastly larger energy for cleavage at the (111) M layer than at the (111) L, M, L composite layer would be expected since the former involves breaking 12 M-O bonds (for the chosen layer unit cell) as compared to 6 M-O and 4 L-O bonds for the latter. In general, the (111) terminations, whose layers are either pure cation or pure anion, and thus have no intralayer bonding, show the most extensive rearrangements when allowed to relax, as discussed in the following subsection.

B. Surface relaxation

The (111) surfaces show the most extensive atomic rearrangements of the low-index surfaces. The results are presented in the following sections.

1. Mn-terminated (111) surface reconstruction

A snapshot of the final reconstructed atomic configuration of the Mn-terminated (111) surface is shown in Fig. 5, in which the atomic positions are projected onto a plane perpendicular to the layers. (For better visualization, the plotted volume includes eight times the number of atoms in the computational cell, 672 atoms, so that the box that encloses the atoms in the figure is roughly cubic.) Atoms in ideally flat atomic layers would fall on a straight line in this projection. Owing to the Jahn-Teller distortion, however, a similar projection of a slab with bulk-terminated atomic coordinates shows some layer rumpling, particularly the oxygen layers (Fig. 6).

Whereas bulk (111) layers are of three types, namely M, O, and L, M, L (Fig. 6), the reconstructed slab shows a termination layer (LMO) that mixes all three components. The reconstruction may be viewed as a migration of the oxygen atoms in the second layer toward the surface to improve bonding with the terminating M layer; L atoms from (the top sublayer of) the LML layer are then drawn toward the surface

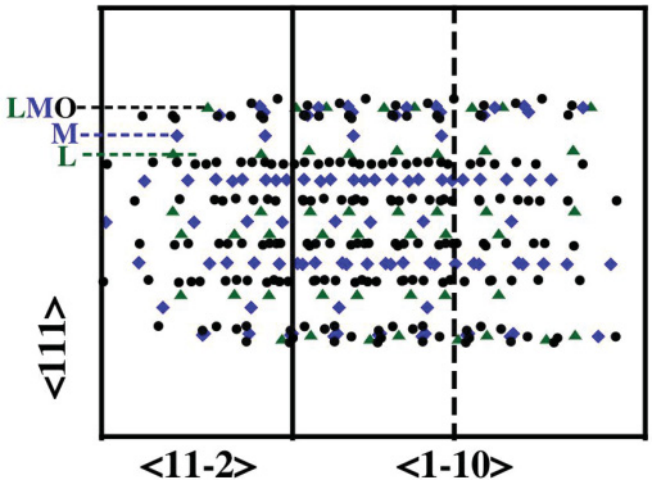

FIG. 5. (Color online) Atomic arrangement of a reconstructed (111) slab, projected onto a plane perpendicular to the layers. LMO termination layers contain a stoichiometric mixture of the components, in contrast to the pure layers of the unreconstructed surface (Fig. 6). The unit-cell box, within layer axes $1\bar{1}0$ and $11\bar{2}$, is rotated by 32 degrees about the 111 axis to obtain the projection.

in the wake of the oxygen atoms to help maintain electrostatic balance.

The atomic rearrangement during reconstruction can be described schematically by the reaction

$$(1/2M_3; O_4; L,M,L; O_4; \ldots) \rightarrow [LM_2O_4; 1/2(M,L); O_4; \ldots], \quad (7)$$

thus, in the reconstructed surface, a mixed LMO layer of stoichiometric composition is superposed on a slab with the (L, M, L) termination [cf. sequence (2)]. We note that this LMO layer bears a negative charge, since Mn atoms in this layer are predominantly trivalent, as described below.

A planar projection of the reconstructed LMO termination layer is shown in Fig. 7. The Mn ions are coordinated in distorted square-planar complexes, with mutual edge and

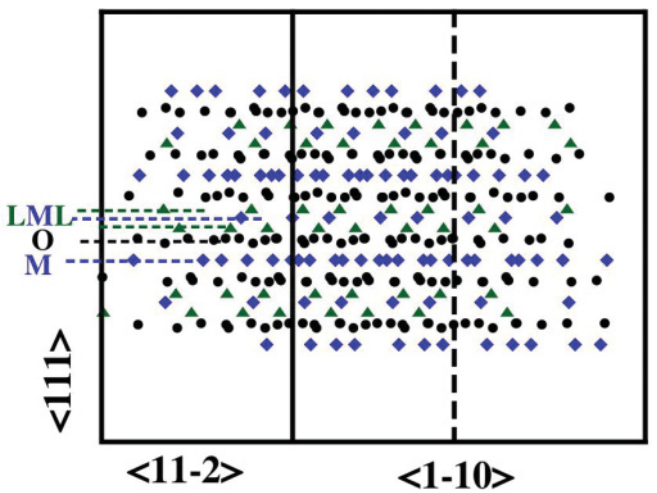

FIG. 6. (Color online) Atomic positions projected onto a plane perpendicular to the layers of a (111) slab, based on simulated bulk atomic structure. The slab exemplifies layer sequence (1) in the text.

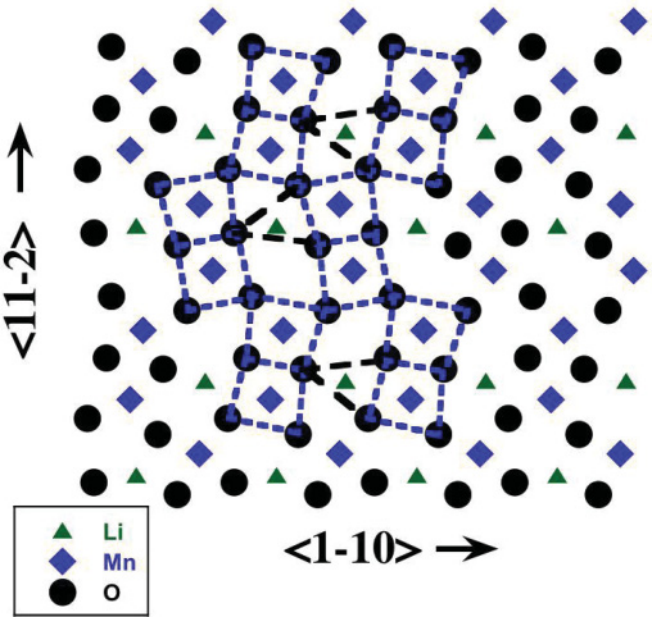

FIG. 7. (Color online) Projection of atomic positions of LMO termination layer of a reconstructed (111) surface. Mn ions display square-planar coordination and Li ions triangular coordination.

corner sharing. The Li ions are threefold-coordinated. The square-planar configuration is favorable for trivalent Mn from a crystal-field viewpoint since the $e_g(3z^2 - r^2)$ orbital lobes pointing into the vacuum are unconstrained by a ligand. The lobes pointing into the slab, however, are constrained by the adjacent ML layer atoms, which may be responsible for the relatively large spacing (about 0.2 nm) of the LMO and ML layer, relative to interlayer spacings in the interior of the slab (cf. Figs. 5 and 6, discussed below). Thus, with the observed separation of the LMO and ML layers, the closest cation-cation separation is of order 0.28 nm, consistent with cation-cation separations in the bulk.

2. Other (111) terminations

The driving force for reconstruction of other (111) terminations is lower than that for the Mn-layer termination, and only for the Mn termination are intermixed LMO layers such as those shown in Fig. 7 predicted. Some features of the reconstructed Mn-terminated (111) surface are nevertheless also observed in the other terminations. For the surface derived from cleavage at the (L,M,L) layer, the surface Li ions are coordinated only to three oxygen ions. These Li ions are found to relax toward the adjacent oxygen plane, to form almost planar threefold-coordinated Li-O complexes, reminiscent of Fig. 7. In the case of the O-terminated (111) surface, some of the subsurface Mn occur in fourfold-coordinated configurations. Unlike in the Mn-terminated surface, however, these complexes are not square planar, but highly distorted tetrahedra. In both cases, however, the fourfold-coordinated Mn are trivalent.

C. Surface coordination numbers

The extensive atomic rearrangement of the Mn-terminated (111) surface is driven in part by the low surface Mn-ion

TABLE I. Coordination numbers for undercoordinated ions near a $LiMn_2O_4$ surface. Bulk coordination numbers are shown in the second column. Oxygen is bonded both to Mn and Li, as indicated in the bottom row.

Orientation termination	(bulk)	(001) MO	(001) L	(110) MO	(110) LMO	(111) LMO	(111) O	(111) ML
Mn	6	4;5	5	3	4,5	4	4;5	3
Li	4	3	2	3	2;3	3	3	3
O	3M,1L	2M;2M,1L	3M;2M,1L	3M;2M,1L;2M	2M;2M,1L	2M,1L;2M,2L	2M;2M,1L;3M	2M,1L;3M

coordination number of 3. The Mn coordination number of the reconstructed surface is raised to 4, and that of Li to 3.

Mn coordination numbers of 3 are found in two other interfaces, namely the MO-terminated (110) surface and the (M,L)-terminated (111) surface. Despite the relatively high energy of such configurations, the simulated room-temperature thermalization of these surfaces by molecular dynamics did not yield any increase in the Mn coordination. The undercoordinated ionic environments for the various surfaces simulated in this work are listed in Table I.

D. Oxidation states

A consequence of the lowered coordination is reduced average Mn oxidation states of near-surface Mn ions, relative to the bulk, for all orientations and terminations simulated in this work. Most surface Mn ions with fourfold or fivefold coordination are predicted to be trivalent, and, for threefold-coordinated Mn, divalent states are also found. The results for the seven different orientation-termination combinations treated are listed in Table II.

E. Surface energy

The surface energy, γ, is defined as the difference between bulk and (relaxed) slab energy, per unit surface area. Results for the surface energies calculated in this work are shown in Table III, along with the ratio of the surface energy to cleavage energy (cf. Fig. 4).

The lowest energy is found for the Li-terminated (001) surface, which is derived from a cleavage that breaks a relatively small number of bonds. The low energy of this surface is consistent with the low energy for the Mg-terminated $MgAl_2O_4$ surface[4] of the prototype spinel. Another relatively low γ surface is the (M,L)-terminated (111) surface, which also is created by breaking a relatively small number of bonds. The LMO-terminated (111) surface, which has the most extensive relaxation, has the lowest ratio of surface to cleavage energy. With both M-O and L-O bonding in the termination plane, the LMO-terminated (110) interface shows the lowest relaxation (and highest ratio of surface to cleavage energy).

The absolute values of γ predicted in this work are somewhat less than those predicted for the corresponding surfaces of $MgAl_2O_4$.[4] The magnitude of the surface energies calculated in this work, however, are closer to those predicted for MnO(001) and (110).[23] The surface energy for the MnO-terminated (001) surface is higher than the value of 0.35 J/m^2 obtained by Ouyang *et al.*[8] This discrepancy may be primarily due to different values of C_v. The use of $C_v = 1/2$ rather than 0[8] increases the coordination deficit at the surface and therefore the surface energy.

V. DISCUSSION

A. Reduced oxidation state of surface Mn

The reduced states of Mn ions near the surface are mostly a consequence of the lower-energy cost of Jahn-Teller distortion in the undercoordinated environment near the surface. This is particularly the case for square-planar coordination in the reconstructed (111) surface, and to a lesser extent for fivefold-coordinated surface complexes. The energy cost of the Jahn-Teller distortion associated with elongating the O-O separation along polar axes of Mn-O_6 octahedra in the bulk, which stabilize the Mn e_g electron of the trivalent ion, is eliminated in the square-planar coordination, since polar-axis oxygens are not present.

Since all Mn ions in the the reconstructed stoichiometric LMO layer of the reconstructed (111) surface (Fig. 5) are trivalent (rather than, say, half trivalent and half tetravalent, as in the bulk), the LMO layer is negatively charged. The surface LMO layer is therefore electrostatically attracted to the positively charged interior of the slab, although cation-cation repulsion keeps the LMO layer separated from the ML layer by about 0.2 nm (Fig. 5).

Nonsquare-planar fourfold-coordinated Mn also occurs [for example, the (001)MO termination and the (110) LMO termination]. Tetrahedrally coordinated Mn tends to favor the divalent oxidation state[24] based on crystal-field splitting. Our

TABLE II. Oxidation state of Mn ions near low-index $LiMn_2O_4$ surfaces, for coordination numbers lower than the bulk value of 6.

CN termination	(001) MO	(001) L	(110) MO	(110) LMO	(111) LMO	(111) O	(111) M,L
3			2+				2+
4	3+			3+	3+	3+	
5		3+				3 + ,4+	

TABLE III. Calculated cleavage energies, E_c, and surface energies, γ, in J/m^2, for low-index lithium manganate surfaces.

Orientation termination	(001) MO	(001) L	(110) MO	(110) LMO	(111) LMO	(111) O	(111) M,L
E_c	1.94	0.75	1.79	1.72	3.76	2.55	1.48
γ	0.98	0.58	1.19	0.99	1.29	1.30	0.85
γ/E_c	0.51	0.77	0.66	0.58	0.34	0.51	0.57

results, however, show Mn in the trivalent rather than divalent states for the fourfold-coordinated complexes at the (001)MO and (110)LMO surfaces. The O-ion cages surrounding the fourfold-coordinated Mn are severely distorted from ideal tetrahedra, so additional splitting may occur, which may help to stabilize the trivalent state.

Although fourfold-coordinated Mn in the divalent state was not found, divalent threefold-coordinated Mn was observed [at the (110)MO and the (111)M,L surfaces]. While divalent Mn is absent from bulk $LiMn_2O_4$, its presence at the surface might facilitate dissolution, since the disproportionation reaction[12] $2Mn^{3+} \rightarrow Mn^{4+} + Mn^{2+}$ would not be required (trivalent Mn dissolves only to a negligible extent). An experimental test of the prediction of divalent Mn ions at the surface of $LiMn_2O_4$ would be useful.

As indicated, threefold-coordinated Mn ions were found at the lowest-energy (110)MO surface. We mention, however, that an interface with a slightly higher energy occurs if a different initial configuration of surface vacancies than in Fig. 3 is adopted. The higher-energy surface would feature (trivalent) fourfold-coordinated Mn, but at the cost of having nonbridging oxygen. This suggests that nonbridging oxygen may be a more unfavorable feature than threefold-coordinated Mn.

B. Mn-terminated (111) surface reconstruction

X-ray reflectometry (XRR) measurements have been made on $LiMn_2O_4$ films with different orientations[25]). The XRR spectra for the (111) orientation required a more elaborate model, with an additional "impurity" layer, than the other low-index orientations to reproduce the data, either for the as-grown films or after soaking with electrolyte. Our calculations showed an extensive rearrangement, relative to the bulk-terminated surface, for the Mn termination, but less pronounced rearrangements for the other terminations considered [(L,M) and O terminations]. It is tempting to associate the simulated Mn-terminated (111) surface reconstruction with the behavior observed in XRR, however the Mn termination is not the one with the lowest surface energy (Table III).

Because of its relatively high energy, the significance of the reconstructed Mn-terminated (111) surface remains in question. The large decrease in the Mn-terminated (111) surface energy for the reconstructed surface, relative to the cleavage energy, indicates that the driving force for reconstruction of such a surface would be strong. That the reconstruction can be accomplished by a rearrangement that results in square-planar Mn coordination, with the three components mixed in stoichiometric proportions, appears not to have been previously noticed.

The reconstruction of the Mn-terminated (111) surface may lead one to hypothesize that all Mn-terminated surfaces must also contain oxygen in the termination layer for stable bonding. One may wonder, for example, whether layer mixing at the ML-terminated (111) surface would occur, in which O migrates to the surface, to improve the coordination of the surface-layer Mn ions. Such a reconstruction, however, was not observed in our room-temperature molecular-dynamics annealing simulations. It is possible that higher-temperature annealing simulations would yield a different reconstruction.

C. Implications for dissolution

Classical dissolution (and crystal growth) models[26] generally assume that dissolution (and growth) occurs primarily in steps, and is essentially negligible for flat surfaces. Our models predict low coordination numbers and oxidation states at the surface, relative to the bulk of $LiMn_2O_4$. Significant dissolution rates may require even larger coordination deficits than occur at the nominally flat surfaces addressed in this paper. Such larger coordination deficits, including nonbridging oxygen, occur, for example, at steps, pits, dislocations, and edges. Consider, for example, an event at a flat surface in which a neighboring Mn^{2+} and an O^{2-} ion dissolve. We have found (Table I) that Mn has a minimum coordination number of 3 and oxygen a minimum coordination number of 2. If the two ions are bonded to each other, the total number of (M-O) bonds of the dissolving pair with the substrate that must be broken for dissolution is at least 3. In the presence of defects, such as steps, however, the required number of bonds could be lowered. Perhaps only when the number of bonds with the substrate to be broken is as low as 2 is the dissolution rate for such an M-O complex significant. Further work is necessary to explore this hypothesis.

VI. CONCLUSIONS

We consider the following results of the GGA + U simulations of lithium manganate surfaces presented in this paper to be noteworthy:

(i) The Mn-terminated (111) interface is predicted to reconstruct so as to form a top layer in which the three components are mixed in stoichiometric proportions, and the Mn is square-planar coordinated.

(ii) All of the terminations and orientations showed an average surface-Mn oxidation state reduced relative to the bulk.

(iii) Surface-Mn coordination numbers vary between 3 and 5; the oxygen coordination number (bonds to Mn) is no less than 2 at flat surfaces. The threefold-coordinated surface Mn is divalent.

(iv) The lowest-energy surface is Li-terminated (001), consistent with the lowest-energy surface for $MgAl_2O_4$, Mg-terminated (001).

ACKNOWLEDGMENTS

The submitted manuscript has been created by UChicago Argonne, LLC, Operator of Argonne National Laboratory ("Argonne"). Argonne, a US Department of Energy Office of Science laboratory, is operated under Contract No. DE-AC02-06CH11357. This work was supported at Argonne by the Office of FreedomCar and Vehicle Technologies [Batteries for Advanced Transportation Technologies (BATT) Program], US Department of Energy. This research used resources of the National Energy Research Scientific Computing Center, which is supported by the Office of Science of the US Department of Energy under Contract No. DE-AC02-05CH11231. We also gratefully acknowledge use of the Fusion cluster in the Laboratory Computing Resource Center at Argonne National Laboratory.

[1]H. Yang, S. Amiruddin, H. J. Bang, Y. K. Sun, and J. Prakash, J. Indust. Eng. Chem. **12**, 12 (2006).
[2]F. Jiao, J. Bao, A. H. Hill, and P. G. Bruce, Angew. Chem. Int. Ed. **47**, 1 (2008).
[3]M. J. Davies, S. C. Parker, and G. W. Watson, J. Mater. Chem. **4**, 813 (1994).
[4]C. M. Fang, S. C. Parker, and G. de With, J. Am. Ceram. Soc. **83**, 2082 (2000).
[5]N. J. van der Laag, C. M. Fang, G. de With, G. A. de Wijs, and H. H. Brongersma, J. Am. Ceram. Soc. **88**, 1544 (2005).
[6]F. Zhou, M. Cococcioni, C. A. Marianetti, D. Morgan, and G. Ceder, Phys. Rev. B **70**, 235121 (2004).
[7]C. Y. Ouyang, S. Q. Shi, and M. S. Lei, J. Alloys Compd. **474**, 370 (2009).
[8]C. Y. Ouyang, X. M. Zeng, Z. Sljivancanin, and A. Baldereschi, J. Phys. Chem. C **114**, 4756 (2010).
[9]G. Kresse and J. Furthmueller, Comput. Mater. Sci. **6**, 15 (1996).
[10]G. Kresse and J. Furthmuller, Phys. Rev. B **54**, 11169 (1996).
[11]G. Kresse and D. Joubert, Phys. Rev. B **59**, 1758 (1999).
[12]J. C. Hunter, J. Solid State Chem. **39**, 142 (1981).
[13]R. Benedek, M. M. Thackeray, and A. van de Walle, J. Mater. Chem. **20**, 369 (2010).
[14]H. Liu and D. Tang, Russian J. Electrochem. **45**, 762 (2009).
[15]P. W. Tasker, J. Phys. C **12**, 4977 (1979).
[16]C. Nogueira, J. Phys. Condens. Matter **12**, R367 (2000); D. Wolf, Phys. Rev. Lett. **68**, 3315 (1992).
[17]J. G. Fripiat, A. A. Lucas, J. M. Andre, and E. G. Derouane, Chem. Phys. **21**, 101 (1977).
[18]C. Franchini, V. Bayer, R. Podloucky, G. Parteder, S. Surnev, and F. P. Netzer, Phys. Rev. B **73**, 155402 (2006).
[19]D. Kramer and G. Ceder, Chem. Mater. **21**, 3799 (2009).
[20]J. Ciston, A. Subramanian, D. M. Kienzle, and L. D. Marks, Surf. Sci. **604**, 155 (2010).
[21]Y. Wang and J. P. Perdew, Phys. Rev. B **44**, 13298 (1991).
[22]M. Nakayama and M. Nogami, Solid State Commun. **150**, 1329 (2010).
[23]V. Bayer, C. Franchini, and R. Podloucky, Phys. Rev. B **75**, 035404 (2007).
[24]J. A. Saint, M. M. Doeff, and J. Reed, J. Power Sources **172**, 189 (2007).
[25]M. Hirayama, N. Sonoyama, M. Ito, M. Minoura, D. Mori, A. Yamada, K. Tamura, J. Muzuki, and R. Kanno, J. Electrochem. Soc. **154**, A1065 (2007).
[26]P. M. Dove, N. Han, and J. J. D. Yoreo, Proc. Natl. Acad. Sci. USA. **102**, 15357 (2005).